Geomechanics and Engineering, *Vol. 38, No. 2 (2024) 205-214*
https://doi.org/10.12989/gae.2024.38.2.205

Application of electrical resistivity for assessing characterizations of frozen and unfrozen soils

Dae-Hong Min[a] and Hyung-Koo Yoon*

Department of Construction and Disaster Prevention Engineering, Daejeon University, Daejeon 34520, Republic of Korea

(*Received April 15, 2024, Revised July 15, 2024, Accepted July 16, 2024*)

Abstract. Permafrost refers to the condition where the ground is frozen. It is crucial to review and evaluate the ground's characteristics before construction. In this study, electrical resistivity surveying is chosen as the investigative technique to apply and illustrate the results on the state of permafrost ground and to summarize its applicability. Field experiments are conducted in the Yeoncheon area of South Korea, which has a freezing index of 522.6°C·days. The target area is categorized into two ground conditions: the first where the original ground freezes, and the second involves excavating the original ground up to a depth of 3 meters, backfilling it, and then artificially injecting fluid. Thus, frozen ground conditions are simulated under both natural and artificial circumstances. Electrical resistivity surveys are performed under both above-freezing and sub-zero temperature conditions, with the experiments conducted at sub-zero temperatures revealing relatively more high-resistivity zones due to the temperature conditions. In this area, the distribution of soil moisture content is also investigated using the Time Domain Reflectometry (TDR) technique. It is observed that the ground into which water is artificially injected had a relatively higher moisture content, although the difference is minor. Finally, a 3D map of the target ground is constructed based on the measured electrical resistivity values, and through this, the distribution of porosity, a crucial design parameter, is also depicted. This research demonstrates that the electrical resistivity technique can effectively evaluate the state of frozen and unfrozen ground and further suggests that it can detailed extract the characteristics of the target ground.

Keywords: 3D map; electrical resistivity; frozen ground; porosity; time domain reflectometry

1. Introduction

Permafrost occurs when ground temperatures drop below the freezing point of water due to low atmospheric temperatures, predominantly in cold, high-latitude regions (Tang *et al.* 2020, Wang *et al.* 2020, Chen *et al.* 2021). It is divided into two main components: the permafrost layer and the active layer. The permafrost layer is a stratum that remains continuously frozen due to the extremely low surrounding temperatures (Byun *et al.* 2014, Shwan 2023, Zamani *et al.* 2023). In contrast, the active layer refers to the surface layer that is not permanently frozen, with temperatures fluctuating above and below freezing, leading to seasonal thawing and refreezing. Accurate assessment of the permafrost, including both the active layer and its internal state, is essential for predicting ground behavior, thereby enabling appropriate design and construction practices.

Electrical resistivity surveying is a non-destructive method that measures ground resistance by generating an artificial electric field and calculating the ratio of injected current to the resulting voltage (Kang *et al.* 2022, Lee *et al.* 2022, Olabode and San 2023, Song *et al.* 2023). This technique offers the advantage of providing detailed insights into the ground's internal structure, making it extensively used to explore the subsurface based on electrical properties. According to Hauck and Kneisel (2008), electrical resistivity is employed to observe the condition of glacial rocks, glacial sediments, and ice in cold regions, enabling the quantification of permafrost's extent and scale. However, it requires maintaining good grounding of both the ground and electrodes during measurements and vigilance against the significant impact of artificial noise from surrounding layers. Fortier *et al.* (2008) implemented electrical resistivity surveying in Canada, differentiating between permanent and semi-permanent permafrost. Their findings revealed stark differences in electrical resistivities—30,000 ohm-meters for permanent permafrost and 1,000 ohm-meters for semi-permanent permafrost—attributable to variations in moisture content distribution within the area. Similarly, Kneisel *et al.* (2008) performed studies in Canada, creating a depth-specific electrical resistivity distribution map and evaluating the thaw depth of permafrost and thawing characteristics of permafrost road foundations. Their research produced tomography results from the electrical resistivity measurements and recorded subsidence due to thawing at a depth of 0.85 meters. It was observed that current flow is influenced by ambient temperature; a decrease in temperature leads to reduced ion activity and, consequently, increased resistance. This indicates that measured values can fluctuate with changes in surrounding temperature (Marrah *et al.* 2023), despite no alteration in the ground's condition, necessitating careful consideration by experimenters (Jung *et al.* 2015). Ground

*Corresponding author, Associate Professor
E-mail: hyungkoo@dju.ac.kr
[a]Ph.D. Candidate

ISSN: 2005-307X (Print), 2092-6219 (Online)

temperature is crucial for precise electrical resistivity measurements, and techniques for adjusting measured resistance based on temperature are in use.

In this study, we utilized electrical resistivity methods to assess the behavior of permafrost regions, with the goal of obtaining accurate electrical resistivity profiles by adjusting for temperature influences, drawing on insights from prior research. Accordingly, we detailed the fundamental principles of electrical resistivity surveying and outlined the methods for temperature compensation. We also described the environmental conditions and the measurement techniques employed at the field experiment sites. Ultimately, the study involved comparing electrical resistivity values measured in both frozen and unfrozen ground to discuss their practical utility.

2. Background theory

2.1 Electrical resistivity survey

Electrical resistivity survey is performed on the assumption that the ground acts as a conductor (Park *et al.* 2017). This method involves injecting a specific current and then measuring the voltage that emerges as a result. The resistance is determined using the current and voltage measurements, and the calculated resistance can vary based on factors such as the cables used, the shape of the electrodes, and the connection method. This variation occurs even within the same type of ground, depending on the measurement technique employed. Consequently, it is essential to convert the measured values to the ground's inherent electrical resistance value. This inherent value is referred to as electrical resistivity. Measuring the ground's inherent electrical resistivity directly is challenging; therefore, we typically measure the apparent electrical resistivity and use it as a proxy for the actual resistivity value. Electrical resistivity (ρ, Ω·m) is adjusted for by applying a distance factor to the measured resistance (R, Ω), as depicted in Eq. (1). The distance factor is selected based on the electrode array method used.

$$\rho = \lambda \cdot R \tag{1}$$

where, λ represents the distance factor, which varies according to Wenner, Schlumberger, and dipole-dipole arrays.

2.2 Temperature compensated method

The ions constituting electricity exhibit varying levels of activity depending on the temperature, leading to changes in resistance values as the ions move. The ground temperature influences ion mobility, necessitating temperature compensation to obtain reliable electrical resistivity measurements. Keller and Frischknecht (1966) proposed a method for temperature compensation, using the electrical resistivity value measured at 18°C (ρ18) as a reference, as indicated in Eq. (2). This method utilizes the measured temperature and the corresponding electrical resistivity at that temperature as input values.

$$\rho_T = \frac{\rho_{18}}{1+\alpha(T-18)} \tag{2}$$

Here, T denotes the ground temperature, and ρ_T shows the electrical resistivity measured at that temperature. Furthermore, α is introduced as a constant value, set at 0.0025. It's important to note that the value of α can differ based on the electrodes and array methods used for measuring electrical resistivity. For a detailed discussion on this topic, the study by Jung *et al.* (2015) is recommended as a valuable resource.

2.3 Interpolation method

In this study, the interpolation method applied to the unknown spatial areas is kriging. Kriging is a method of interpolating data for nearby unknown spatial areas based on correlations with the original data using a variogram. A variogram is divided into three components: Sill, Nugget, and Range, which represent the original data variance, the intercept, and the distance of influence, respectively. The appropriate variogram is selected through the fit between the experimental model plotted from the experimental results and the theoretical model. In this study, the spherical model was applied.

3. Methodlogy

The study aimed to understand the variations in electrical resistivity due to freezing by constructing both natural and artificial grounds. The original terrain of the area is composed of a gravel and silt alluvial layer, with the groundwater level situated below 3 meters. The term "natural ground" refers to the ground in its original state. As depicted in Fig. 1(a), a 3 m x 6m area (width x length) was designated for the installation of electrical resistivity electrodes. For the artificial ground, illustrated in Fig. 1(b), the original terrain up to a depth of 3 meters from the surface was mixed using an excavator, and water was then sprayed across the entire area using a high-pressure hose. This process of mixing and watering was designed to induce a significant freezing effect, thereby creating a discernible difference in the freezing states between the natural and artificial grounds, which in turn aids in the comparison of electrical resistivity. Both the natural and artificial grounds utilized the Wenner array configuration for measuring electrical resistivity, with an electrode spacing set at 1 meter. This spacing was chosen to optimize the resolution capability relative to the area covered, achieving a resolution depth of 0.5 meters. The survey lines are marked with blue lines in Fig. 1, with the horizontal directions labeled as L1, L2, and L3, each extending 3 meters in length, making up a total of three lines. The vertical directions, labeled as L4, L5, and L6, each extend 6 meters in length. The survey lines were strategically placed at the outer boundaries of the measurement area to facilitate a comprehensive exploration of the ground, with each line intersecting orthogonally at positions that divide the area in half.

The Time Domain Reflectometry (TDR) experiment was conducted to measure the moisture content in both natural and artificial grounds, with its locations marked in black on Fig. 1.

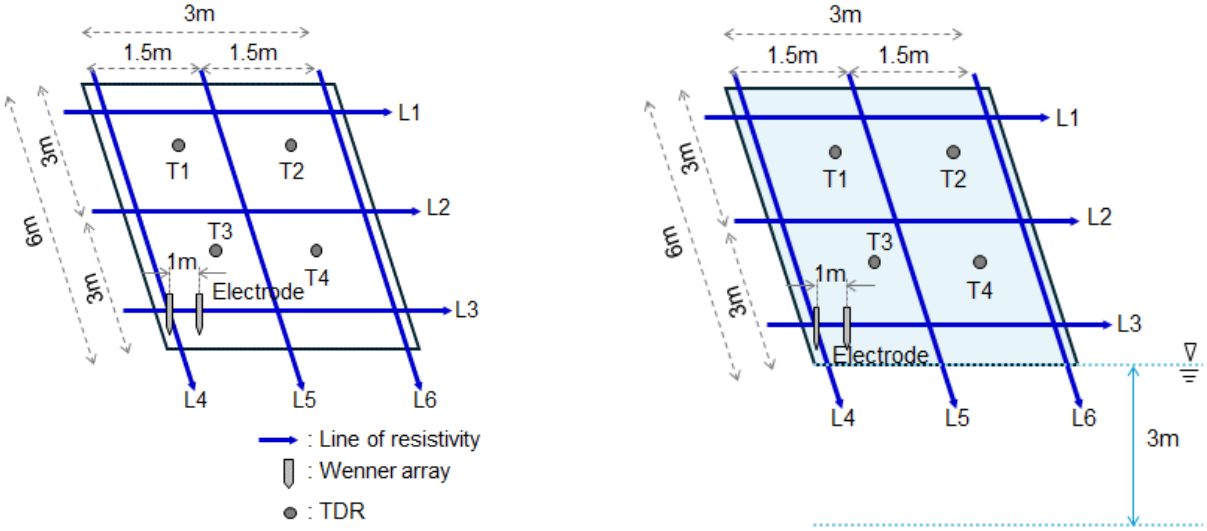

Fig. 1 Schematic drawing of measurement in field with electrical resistivity and time domain reflectometry (TDR): (a) natural ground and (b) artificially constructed ground

To prevent interference from the electrical resistivity currents, TDR probes were placed in the vacant spaces outside the survey lines. The electrical resistivity and TDR experiments were performed twice, at different times, and are referred to as the first and second experiments. The first experiment occurred in December, from 10:00 to 15:00. During this time, the average atmospheric temperature in the area ranged from a minimum of 5°C to a maximum of 8°C, based on data from the Korea Meteorological Administration (KMA). The second experiment was carried out in February of the following year, within the same timeframe of 10:00 to 15:00 as the first experiment. Contrary to the first period, temperatures were in the sub-zero range, from -10°C to -5°C.

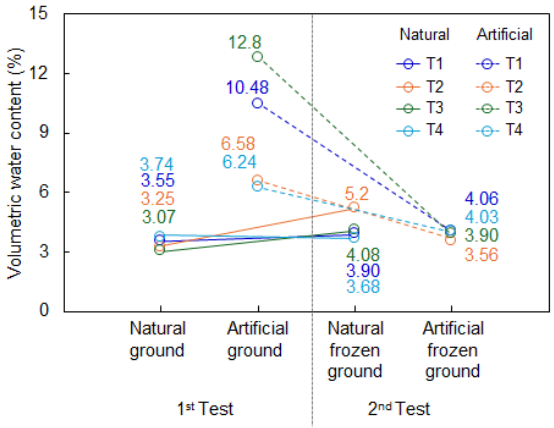

Fig. 2 Results of time domain reflectometry. The volumetric water content is obtained through measured voltage with correlation equation

4. Result

4.1 TDR

The results of the Time Domain Reflectometry (TDR) experiments conducted on both natural and artificial grounds are depicted in Fig. 2. These results categorize the moisture content by ground type and illustrate changes across the experimental periods. The first period featured an average atmospheric temperature above the freezing point, indicating unfrozen ground conditions. Conversely, the second experiment was carried out under sustained sub-zero temperatures, visually confirming the ground's frozen state. Consequently, the term "frozen" was designated for both natural and artificial grounds during the second experiment. For the natural ground, moisture content measurements during the first experiment for T1, T2, T3, and T4 were 3.55%, 3.25%, 3.07%, and 3.74%, respectively, yielding an average moisture content of 3.40%. In the second experiment, the moisture contents for T1, T2, T3, and T4 were 3.90%, 5.20%, 4.08%, and 3.68%, respectively, resulting in an average moisture content of 4.21%, which is higher than that recorded in the first experiment. Regarding the artificial ground, the moisture content during the first period for T1 through T4 was 10.48%, 6.58%, 12.80%, and 6.24%, respectively, with an average moisture content of 9.02%. The moisture content difference between the natural and artificial grounds was 5.62%, with the artificial ground displaying approximately 2.6 times higher moisture content, likely a result of artificial ground. In the second experiment, the moisture content for the artificially frozen ground was 4.06%, 3.56%, 3.90%, and 4.03%, respectively, with an average moisture content of 3.88%. This is 5.13% lower than the average moisture content of the artificial ground in the first experiment. The relatively lower moisture content observed in the second experiment is attributed to the solidification of pore water due to freezing, suggesting that the frozen state can be indirectly inferred from the TDR-measured moisture content.

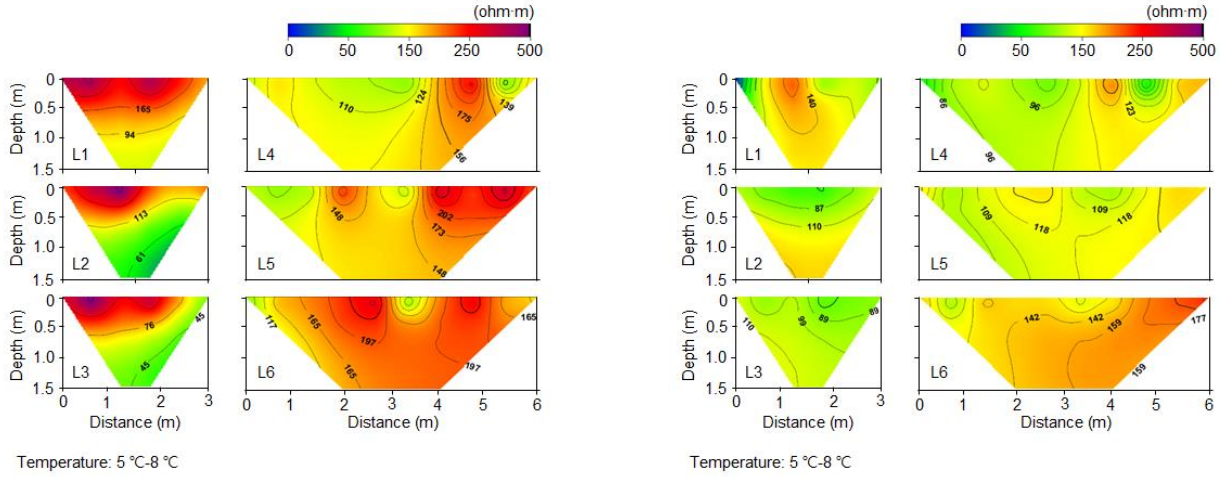

(a) (b)

Fig. 3 Results of 1st experiment through electrical resistivity survey for unfrozen condition: (a) natural ground and (b) artificially constructed ground

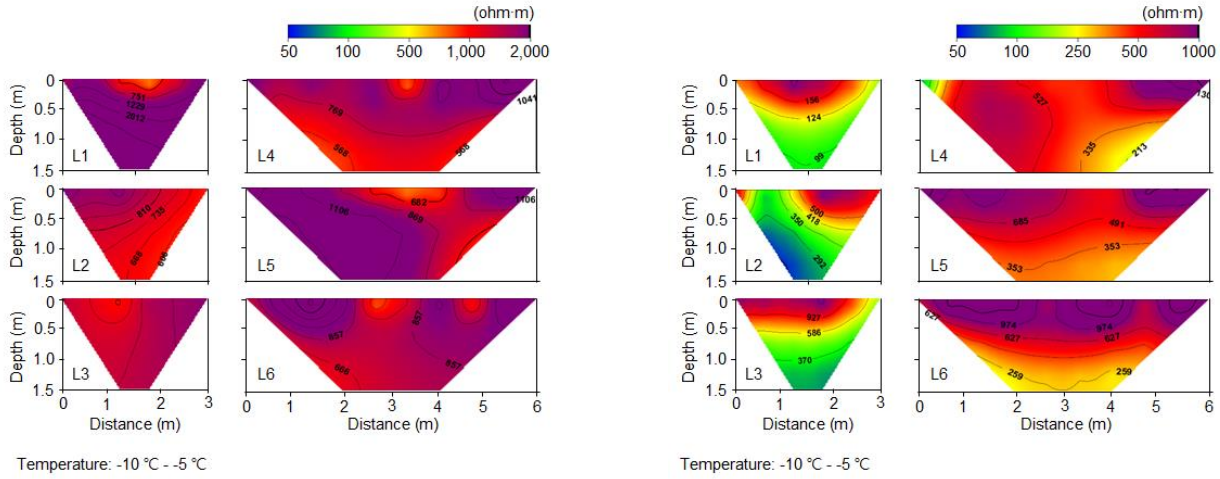

(a) (b)

Fig. 4 Results of 2nd experiment through electrical resistivity survey for frozen condition: (a) natural ground and artificially constructed ground

4.2 Electrical resistivity

Fig. 3 displays the results of the initial electrical resistivity survey conducted on both natural and artificial grounds using the Wenner array, with the resistivity values represented as contour lines. Fig. 3(a) illustrates the findings for the natural ground, showing a comprehensive electrical resistivity range from 0 to 500 Ω·m and revealing the maximum exploration depth of 1.5 m, which corresponds to the 1m electrode spacing of the Wenner array. L1, L2, and L3 show a high resistivity zone ranging from 300 to 500 Ω·m from the surface to a depth of 0.5-0.7 m, whereas the depth ranges of 0.7 m to 1.5 m exhibits a relatively low resistivity zone of 100 to 150 Ω·m. L4, L5, and L6 do not distinctly delineate the boundary between low and high resistivity zones, presenting an overall electrical resistivity range of 110 to 220 Ω·m. The intersection points of L4, L5, and L6 are expected to display values consistent with adjacent areas, yet they seem to obscure the boundaries due to reduced resolution. Fig. 3(b) presents the findings from artificial ground, employing the same electrical resistivity range as that of the natural ground. It reveals a uniformly low resistivity zone of 100-150 Ω·m extending from the surface down to a depth of 1.5 m. L1, L2, and L3 show an average resistivity of 120 Ω·m from the surface to a depth of 0.7 m, which is lower than the natural ground's average of 420 Ω·m for the same depth range. The depth ranges of 0.7-1.5 m maintains a similarly low average resistivity of 110 Ω·m. In contrast to the natural ground, there is no high resistivity zone near the surface, and the boundary between high and low resistivity zones is not discernible. The results for L4, L5, and L6 indicate an electrical resistivity range of 90-160 Ω·m across the entire depth, showing resistivity values that are 20-60 Ωm lower than those of the natural ground. This suggests that the artificial ground exhibits relatively low resistivity values throughout, likely due to an artificial increase in moisture content and porosity from ground mixing, as reflected in the moisture content findings in Fig. 2.

Fig. 4 presents the results of the second experiment, showcasing an overall electrical resistivity range that is fourfold that of the first experiment, spanning from 50 to 2,000 Ω·m. Fig. 4(a) illustrates the electrical resistivity image for the naturally frozen ground, with measurements ranging from a minimum of 600 Ω·m to a maximum of 2,000 Ω·m. L1, L2, and L3 displayed a high resistivity zone within the range of 600-2,000 Ω·m, unlike the first experiment, which showed no low resistivity zones and exhibited up to 20 times higher resistivity compared to the first experiment. L4, L5, and L6 revealed a high resistivity zone ranging from 600-1,100 Ω·m, indicating up to 900 Ω·m higher resistivity compared to the natural ground. Electrical resistivity is inversely related to temperature, meaning resistivity values increase as temperature decreases. Conducted at sub-zero temperatures of -10 to -5°C, the second experiment appears to show higher resistivity values at all depths, being up to 15°C lower than the average atmospheric temperature of the first experiment. Fig. 4(b) displays the results for the artificially frozen ground, showing a range approximately 50% lower than that of the naturally frozen ground in Fig. 4(a). This indicates that, despite being in a frozen state, the ground exhibited relatively low resistivity zones due to the influence of moisture content. In Fig. 4(b), L1, L2, and L3 exhibit a high resistivity zone ranging from 500-900Ω·m down to a depth of 0.5-0.7 m, transitioning to a low resistivity zone of 100-200 Ω·m below 0.7 m. The boundary between high and low resistivity zones follows a similar trend to the results of the first experiment. Additionally, areas L4, L5, and L6 from a high resistivity zone of 500-900 Ω·m to a low resistivity zone of 200-300 Ω·m around a depth of 0.7-0.8 m, indicating higher resistivity compared to the first experiment's results, likely due to the lower ground temperature. Therefore, in contrast to Fig. 4(a), the overall absence of high resistivity zones suggests that the influence of temperature and moisture content. Consequently, the freezing depth is estimated to extend up to 0.5-0.7 m, where high resistivity zones are present.

5. Discusssion

5.1 Comparison of electrical resistivity in 3D map

The cross-sections of measured electrical resistivity at various locations can be visualized through tomography, which uses the x, y, and z coordinates for three-dimensional modeling. Although tomographic models provide the advantage of detailing information across three axes, they result in discontinuous modeling, unable to deliver electrical resistivity values for the undefined spaces between measurement lines. Within the realm of geostatistics, Kriging is a method that predicts and models these unknown spaces by leveraging the correlation among sample data values, grounded in a variogram that applies distance-related weights. This research employed the Kriging technique on electrical resistivity findings to achieve a model with more continuity than that offered by standard tomography. Fig. 5 displays the Kriging outcomes for spatial predictions based on the electrical resistivity cross-sections of both natural and artificially constructed grounds from the initial experiment, maintaining a consistent electrical resistivity range of 50-200 Ω·m following temperature adjustment. This temperature correction facilitates a strategic comparison of the two terrains through temperature standardization, showcasing the electrical resistivity values for both at an adjusted temperature of 18°C. Fig. 5(a) displays the Kriging spatial prediction results for the electrical resistivity of natural ground from the initial experiment. While the range of electrical resistivity values differs from that shown in Fig. 3(a), the overall trend is similar, indicating a transition from high to low resistivity with increasing depth. The right side of Fig. 5(a) presents a 3D cross-section delineated by depth, where the z-axis signifies depth. The focus on the z-axis aims to elucidate the variation in electrical resistivity values throughout the entire cross-section as depth increases. The depths set for the z-axis are 0 m, 0.5 m, 1.0 m, and 1.5 m. At a surface level of 0m, approximately 70% of the area showed a high resistivity range of 180-200Ω·m, a phenomenon attributed to the low natural moisture content, approximately 3%. At 0. 5 m depth, about 65% of the area demonstrated a high resistivity of 200Ω·m, while at depths of 1.0 m and 1.5 m, over 50% of the area fell within the low resistivity range of 80-110 Ω·m. Fig. 5(b) reveals the Kriging results for artificial ground, exhibiting an overall electrical resistivity range of 80-120Ω·m, which is notably lower compared to natural ground. At a depth of 0m, the electrical resistivity range of 50-100Ω·m encompasses more than 90% of the area, and this range continues across depths of 0.5 m to 1.5 m. Relative to natural ground (Fig. 5(a)), artificial ground (Fig. 5(b)) showed lower electrical resistivity values by 30-100Ω·m at each assessed depth, a consequence of increased artificial moisture content. The application of temperature correction and Kriging analysis successfully demonstrated the influence of moisture content, affirming the capability to detect the impact of moisture within voids via electrical resistivity

Figs. 5(a) and 5(b) exhibited the same electrical resistivity values at the same locations as the actual electrical resistivity measurement results, showing a similar trend with changes in depth. This validated the reliability of the kriging interpolation prediction results.

Fig. 6 shows the kriging results for natural and artificially constructed grounds from the second experiment, akin to Fig. 5, which determined electrical resistivity values via a temperature correction formula. Before temperature correction, the electrical resistivity ranges were 50-2,000 Ω·m for natural ground and 50-1,000 Ω·m for artificially constituted ground, presenting distinct ranges that complicate direct comparisons. Post-temperature correction, both natural and artificially constituted grounds exhibit a unified electrical resistivity range of 50-1,000Ω·m, enabling straightforward comparison and assessment of ground freezing effects. Fig. 6(a) displays the kriging results of electrical resistivity for natural ground, revealing a high resistivity zone up to 800 Ω·m higher than that observed in the first experiment (Fig. 5(a)). Figs. 5(a) and 6(a) depict electrical resistivity

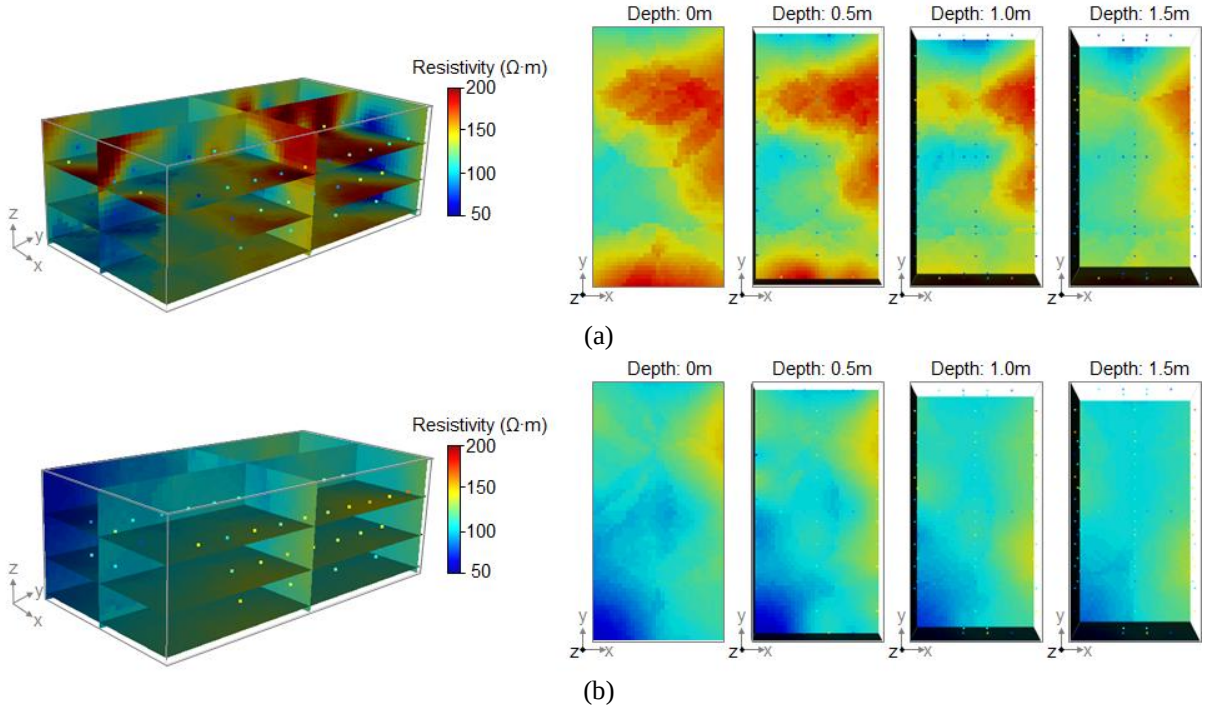

Fig. 5 Kriging modelling with unfrozen condition results: (a) natural ground and (b) artificially constructed ground

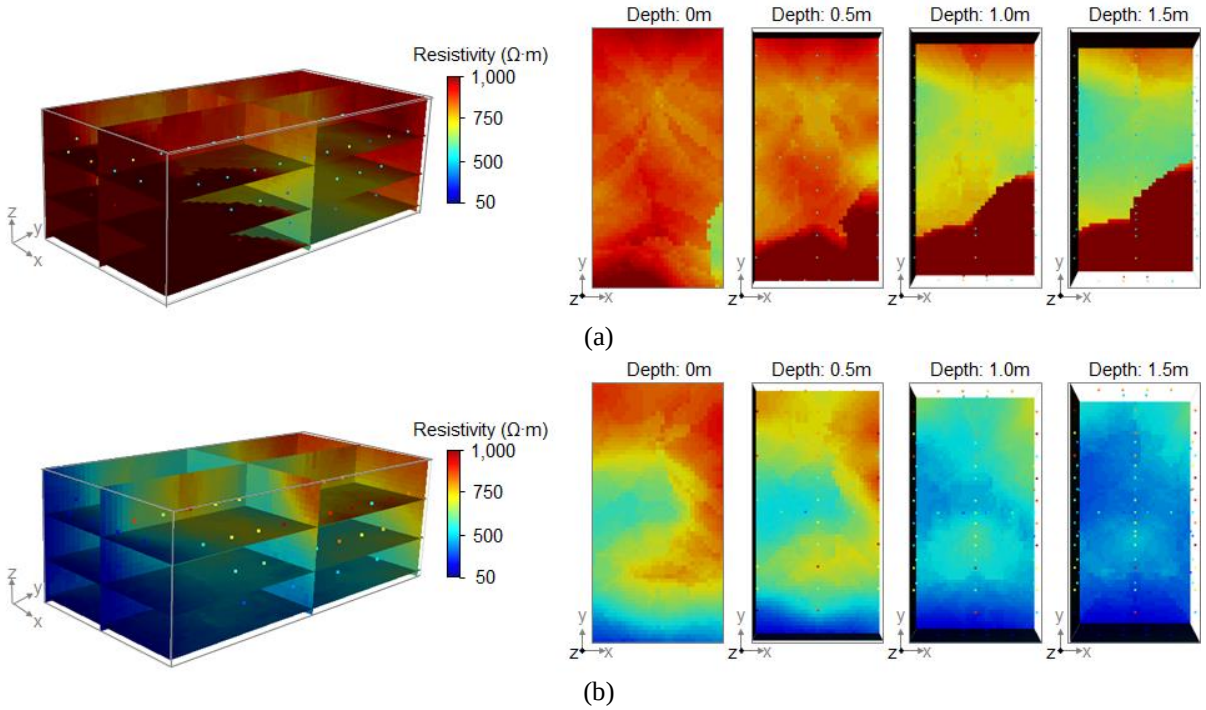

Fig. 6 Kriging modelling with frozen condition results: (a) natural ground and (b) artificially constructed ground

values at 18°C post-temperature correction, allowing for a temperature impact-excluded comparison. At a depth of 0m, the first experiment showed a high resistivity zone peaking at 200 Ω·m, whereas the second experiment revealed a high resistivity zone of 900-1,000 Ω·m covering over 90% of the area, persisting up to a depth of 0.5 m. At depths of 1.0-1.5 m, the first experiment identified a low resistivity zone of 100-160 Ω·m occupying more than 70% of the area, in contrast to the second experiment, which displayed a low resistivity zone ranging from 500-700 Ω·m, also covering over 70% of the area. The trends of electrical resistivity in both experiments were similar, with an expansion in the area of low resistivity zones as depth increased, though the value ranges were approximately five times greater in the second experiment. This trend is attributed to the increase in electrical resistivity up to a depth of 0.5 m in the second

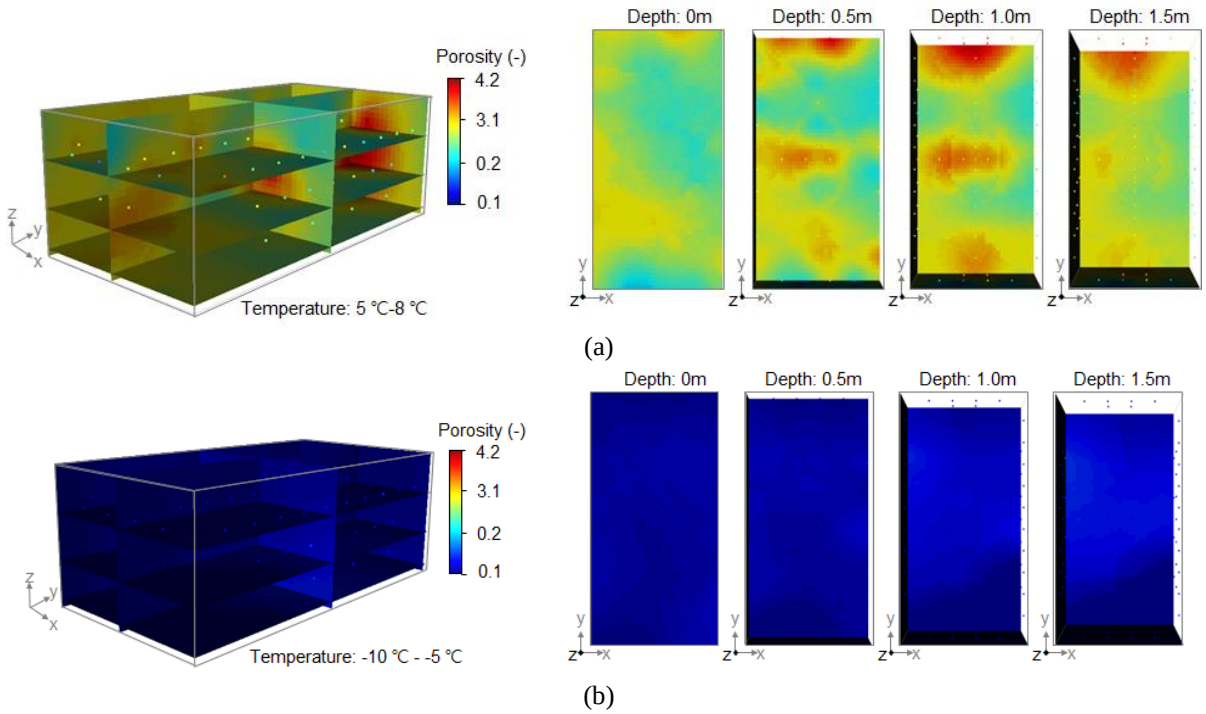

Fig. 7 Kriging modelling of porosity with unfrozen and frozen condition in natural ground: (a) 1st experiment and (b) 2nd experiment

experiment, caused by the freezing of approximately 3% moisture content in the natural ground, with no freezing effect observed beyond a certain depth. Fig. 6(b) presents the kriging results for artificially constituted ground in the second experiment, facilitating an evaluation of freezing effects in comparison to the first experiment. The first experiment (Fig. 5(a)) demonstrated a generally low resistivity zone due to an increase in artificial moisture content, while the second experiment (Fig. 6(a)) showed a high resistivity zone up to 900 Ω·m higher than the first (up to a depth of 0-0.5 m), attributed to the freezing of interstitial water caused by lower ground temperatures. Below a depth of 1.0 m, outside the freezing influence, a low resistivity zone ranging from 50-100 Ω·m emerged, aligning with the original moisture content (6.24-12.8%). These experiments highlight the utility of electrical resistivity in gauging the extent of freezing effects through variations in low temperatures and artificially induced moisture increases. The freezing condition in Fig. 6, like the unfrozen condition in Fig. 5, showed that the actual electrical resistivity values and the kriging results produced comparable images as depth increased.

5.2 3D Modeling of porosity

This study inferred electrical resistivity values based on the degree of freezing and utilized Archie's equation to estimate the changes in porosity resulting from freezing. Archie's equation is presented below, indicating that electrical resistivity is determined by the porosity and constant values.

$$F = \frac{R_w}{R_0} = \alpha \cdot n^{-m} \tag{3}$$

where, F denotes the ratio between Rw and R0, where Rw and R0 represent the electrical resistivity of the current state and the 100% saturated ground, respectively. The symbol n indicates porosity, while α and m serve as shape factors and constants, according to Archie (1942). Typically, α and m values range from 0.62-1.65 and 1.3-2.15, respectively, for common sedimentary and alluvial layers (Carothers 1968, Byun *et al.* 2019), with the median values of 1.13 and 1.72 adopted as the constants for this study. The porosity derived from Archie's equation underwent kriging for 3D modeling, analogous to the process applied to electrical resistivity values.

To facilitate a comparison of porosity before and after freezing, the porosities from the first and second experiments were analyzed, with the findings for the natural ground illustrated in Fig. 7 and for the artificially constituted ground in Fig. 8. Porosity is inversely proportional to electrical resistivity, where higher resistivity is depicted in blue for lower porosity, and lower resistivity in red for higher porosity. Figs. 7(a) and 7(b) showcase the 3D modeled porosity changes due to freezing in natural ground from the first and second experiments, respectively, setting the porosity range consistently at 0.1-0.42. Fig. 7(a) displays the porosity prior to freezing, at a time when the atmospheric temperature is comparatively high, showing an average porosity of 0.27 at depths of 0-0.5 m and a porosity of 0.29 at depths of 0.5-1.5 m. This study observed natural ground trends consistent with general expectations, with porosity increasing with depth, albeit by a small average difference of 0.02. Given the maximum depth of 1.5m, this depth difference appears minor. Fig. 7(b) models the porosity after exposure to sub-zero temperatures, revealing a low porosity range of 0.1-0.11 across all depths.

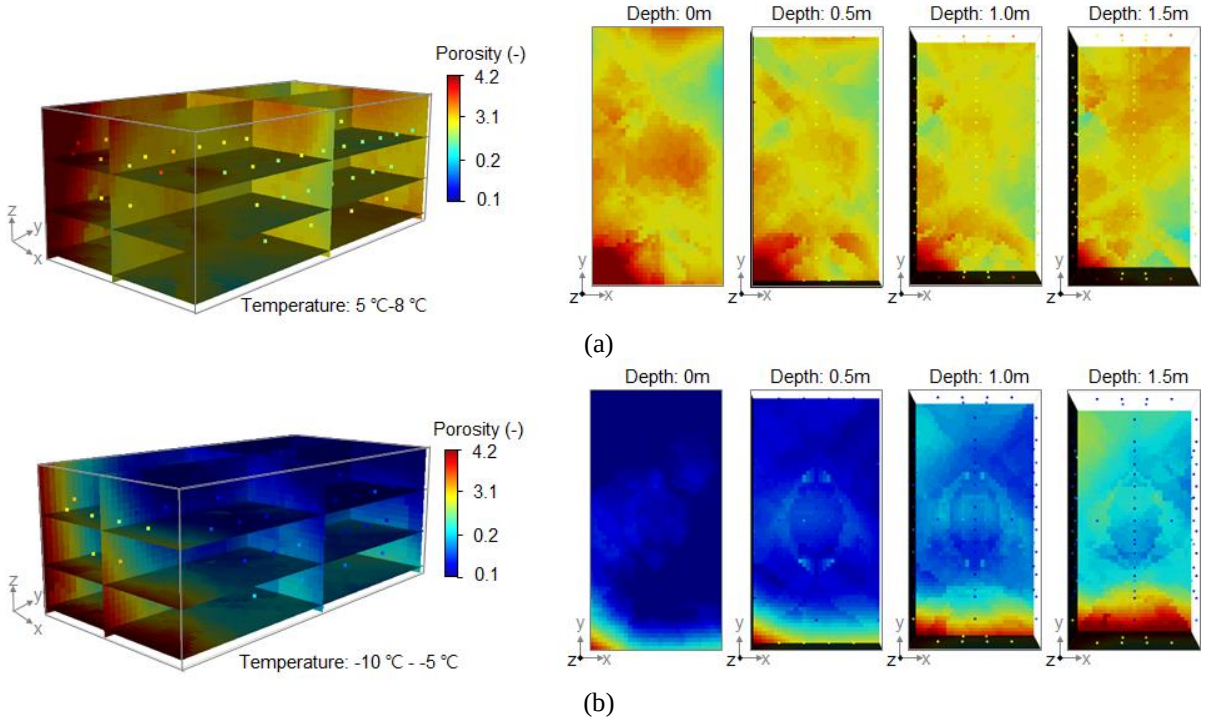

Fig. 8 Kriging modelling of porosity with unfrozen and frozen condition in artificially constructed ground: (a) 1st experiment and (b) 2nd experiment

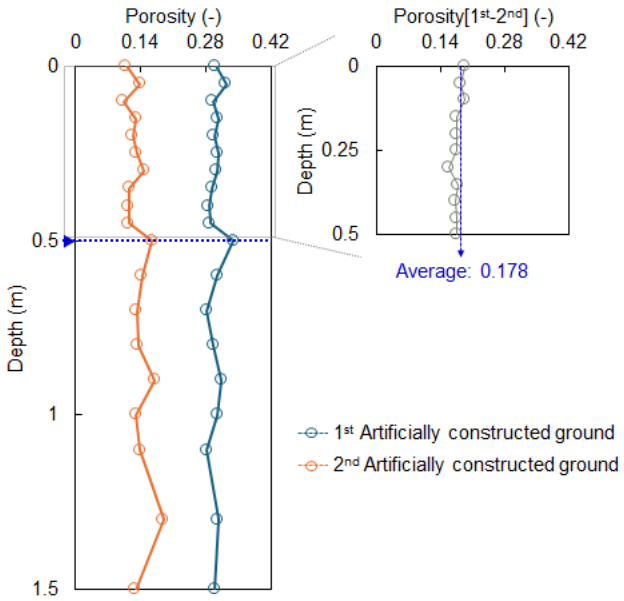

Fig. 9 Detailed porosity profile based on 1st and 2nd experimental results in artificially constructed ground

It is believed that in the second experiment, porosity decreased in certain areas due to approximately 3% of moisture freezing, indicating that changes in porosity are not solely due to complete freezing at all depths but also to the effects of high resistivity.

Fig. 8 models the porosity for artificially constituted ground in both the first and second experiments, maintaining the same porosity range as the natural ground. Fig. 8(a) presents the first experiment's results on artificial ground, showing an average porosity of 0.31 at depths of 0-0.5 m and a porosity of 0.29 at depths of 0.5-1.5 m. The porosity up to a depth of 0.5 m is 0.04 higher than that of the natural ground, suggesting an increase due to artificial disturbance. However, below 0.5 m, the porosity aligns with the natural ground at 0.29, likely indicating compaction effects from the weight of the upper layers after disturbance. Fig. 8(b) displays the calculated porosity post-freezing, with an average porosity of 0.15 at depths of 0-0.5

m and 0.17 at depths of 0.5-1.5 m. The second experiment revealed an average reduction in porosity to 0.16 up to 0.5 m and 0.12 below 0.5 m after freezing, compared to the first experiment. The decreased porosity in the second experiment is attributed to the reduction in gap space due to the freezing of artificial moisture content. The higher porosity below 0.5 m is likely because that depth did not undergo freezing. Fig. 9 extracts the porosity profile graph from the modeling of artificially constituted ground porosity, depicting the graph up to the total depth and the freezing depth. The second experiment shows lower porosity due to high resistivity from freezing. The 0.5m depth, delineating the boundary between high and low resistivity, was analyzed as the freezing depth. The porosity difference up to the freezing depth, as depicted in the right graph up to 0.5 m, averages a difference of 0.178, with the second experiment showing lower values, thus confirming a reduction in porosity due to freezing. Collectively, these results suggest that the degree of freezing can be determined using electrical resistivity, and the reduction in porosity due to freezing can be verified through Archie's equation.

6. Conclusions

In this study, the electrical resistivity technique was employed to observe the behaviors of frozen and unfrozen soils. Experiments were conducted in two distinct ground conditions, and the detailed conclusions of the paper are as follows:

- The ground used for the experiments was categorized into two types. The first type was the natural ground, which freezes naturally due to a decrease in temperature. The second type was modified to facilitate freezing by excavating to a certain depth and artificially applying fluid. The feasibility of using electrical resistivity surveying was assessed under these two ground conditions.
- The measured electrical resistivities were analyzed by categorizing them into above-freezing and below-freezing temperature conditions. In the below-freezing condition, a wider distribution of high-resistivity zones was observed, attributable to the relationship between temperature and resistance. However, the difference in electrical resistivity between the natural and artificially modified grounds was found to be minimal.
- A 3D map was generated using the electrical resistivities measured along the predetermined transects to deduce the conditions of areas. This approach facilitated the detailed extraction of electrical resistivity profiles. Furthermore, a methodology was proposed to offer insights into distinguishing the characteristics of frozen and unfrozen soils by converting resistivity values into porosity.

Acknowledgments

This research was supported by the Basic Science Research Program through the National Research Foundation of Korea (NRF) funded by the Ministry of Education (NRF-2020R1A2C2012113).

References

Archie, G.E. (1942), "The electrical resistivity log as an aid in determining some reservoir characteristics", *T. Am. Inst. Mech. Engineers*, **146**, 54-67. https://doi.org /10.2118/942054-G.

Byun, Y.H., Hong, W.T. and Yoon, H.K. (2019), "Characterization of cementation factor of unconsolidated granular materials through time domain reflectometry with variable saturated conditions", *Materials*, **12**(8), 1340. https://doi.org/10.3390/ma12081340.

Byun, Y.H., Yoon, H.K., Kim, Y.S., Hong, S.S. and Lee, J.S. (2014), "Active layer characterization by instrumented dynamic cone penetrometer in Ny-Alesund, Svalbard", *Cold Reg. Sci. Technol.*, **104**, 45-53. https://doi.org/10.1016/j.coldregions.2014.04.003.

Carothers, J.E. (1968), "A statistical study of the formation factor relation", *Log Anal*., **9**, 13-20.

Cheng, S., Wang, Q., Fu, H., Wang, J., Han, Y., Shen, J. and Lin, S. (2021), "Effect of freeze-thaw cycles on the mechanical properties and constitutive model of saline soil", *Geomech. Eng*., **27**(4), 309-322. https://doi.org/10.12989/gae.2021.27.4.309.

Fortier, R., LeBlanc, A.M., Allard, M., Buteau, S. and Calmels, F. (2008), "Internal structure and conditions of permafrost mounds at Umiujaq in Nunavik, Canada, inferred from field investigation and electrical resistivity tomography", Can. J. Earth Sci., **45**(3), 367-387. https://doi.org/10.1139/E08-004.

Hauck, C. and Kneisel, C. (2006), "Application of capacitively-coupled and DC electrical resistivity imaging for mountain permafrost studies", *Permafrost and Periglacial Processes*, **17**(2), 169-177. https://doi.org/10.1002.

Jung, S.H., Yoon, H.K. and Lee, J.S. (2015), "Effects of temperature compensation on electrical resistivity during subsurface characterization", *Acta Geotechnica*, **10**(2), 275-287. https://doi.org/10.1007/s11440-014-0301-8.

Kang, M., Kim, S., Lee, J. and Choi, H. (2022), "FE model of electrical resistivity survey for mixed ground prediction ahead of a TBM tunnel face", *Geomech. Eng*., **29**(3), 301-310. https://doi.org/10.12989/gae.2022.29.3.301.

Keller, G.V. and Frischknecht, F.C. (1966), "Electrical methods in geophysical prospecting",. https://doi.org/10.1016/S0076-695X(08)60601-8.

Kneisel, C., Hauck, C., Fortier, R. and Moorman, B. (2008), "Advances in geophysical methods for permafrost investigations", Permafrost and periglacial processes, **19**(2), 157-178. https://doi.org/10.1002.

Lee, J.S., Park, J., Kim, J. and Yoon, H.K. (2022), "Study of oversampling algorithms for soil classifications by field velocity resistivity probe", *Geomech. Eng*., **30**(3), 247-258. https://doi.org/10.12989/gae.2022.30.3.247

Marrah, M.Y., Fall, M. and Almansour, H. (2023), "Numerical simulation of ground thermal response in Canadian seasonal frost regions to climate warming", *Int. J. Geo-Eng*., **14**(1), 16. https://doi.org/10.1186/s40703-023-00196-9.

Olabode, O.P. and San, L.H. (2023). Analysis of soil electrical resistivity and hydraulic conductivity relationship for characterization of lithology inducing slope instability in residual soil", *Int. J. Geo-Eng*., **14**(1), 7. https://doi.org/10.1186/s40703-023-00184-z.

Park, C.H., Byun, J.H., Won, K.S., Cho, H.T. and Yoon, H.K. (2017), "Characterization of alluvium soil using geophysical and sounding methods", *Mar. Georesour. Geotec*., **35**(1), 127-135. https://doi.org/10.1080/1064119X.2015.1114545.

Shwan, B.J. (2023), "Microstructural interpretation of effective stress equations for unsaturated sands", *Int. J. Geo-Eng*., **14**(1), 4. https://doi.org/10.1186/s40703-022-00181-8.

Song, S.Y., Kim, B., Cho, A., Jeong, J., Lee, D. and Nam, M.J.

(2023), “Electrical resistivity survey and interpretation considering excavation effects for the detection of loose ground in urban area”, *Geomech. Eng.*, **35**(2), 109-119. https://doi.org/10.12989/gae.2023.35.2.109.

Tang, L., Du, Y., Liu, L., Jin, L., Yang, L.. and, & Li, G. (2020), “Effect mechanism of unfrozen water on the frozen soil-structure interface during the freezing-thawing process”, *Geomech. Eng.*, **22**(3), 245-254. https://doi.org/10.12989/gae.2020.22.3.245.

Wang, T., Zhou, G., Wang, J. and Wang, D. (2020), “Impact of spatial variability of geotechnical properties on uncertain settlement of frozen soil foundation around an oil pipeline”, *Geomech. Eng.*, **20**(1), 19-28. https://doi.org/10.12989/gae.2020.20.1.019.

Zamani, S., Lajevardi, S.H., Yarivand, A. and Zeighami, E. (2023), “Experimental study of the behavior of square footing on reinforced sand with treated geotextile.”, *Int. J. Geo-Eng.*, **14**(1), 19. https://doi.org/10.1186/s40703-023-00195-w.

IC